DOI: 10.3901/CJME.2015.0925.116, available online at www.springerlink.com; www.cjmenet.com

Voronoi Based Discrete Least Squares Meshless Method for Heat Conduction Simulation in Highly Irregular Geometries

LABIBZADEH Mojtaba

Assistant Professor of Structural Engineering, Civil Engineering Department, Faculty of Engineering, Shahid Chamran University, Ahvaz, Iran

Received June 1, 2015; revised September 11, 2015; accepted September 25, 2015

Abstract: A new technique is used in Discrete Least Square Meshfree(DLSM) method to remove the common existing deficiencies of meshfree methods in handling of the problems containing cracks or concave boundaries. An enhanced Discrete Least Squares Meshless method named as VDLSM(Voronoi based Discrete Least Squares Meshless) is developed in order to solve the steady-state heat conduction problem in irregular solid domains including concave boundaries or cracks. Existing meshless methods cannot estimate precisely the required unknowns in the vicinity of the above mentioned boundaries. Conducted researches are limited to domains with regular convex boundaries. To this end, the advantages of the Voronoi tessellation algorithm are implemented. The support domains of the sampling points are determined using a Voronoi tessellation algorithm. For the weight functions, a cubic spline polynomial is used based on a normalized distance variable which can provide a high degree of smoothness near those mentioned above discontinuities. Finally, Moving Least Squares(MLS) shape functions are constructed using a varitional method. This straight-forward scheme can properly estimate the unknowns(in this particular study, the temperatures at the nodal points) near and on the crack faces, crack tip or concave boundaries without need to extra backward corrective procedures, i.e. the iterative calculations for modifying the shape functions of the nodes located near or on these types of the complex boundaries. The accuracy and efficiency of the presented method are investigated by analyzing four particular examples. Obtained results from VDLSM are compared with the available analytical results or with the results of the well-known Finite Elements Method(FEM) when an analytical solution is not available. By comparisons, it is revealed that the proposed technique gives high accuracy for the solution of the steady-state heat conduction problems within cracked domains or domains with concave boundaries and at the same time possesses a high convergence rate which its accuracy is not sensitive to the arrangement of the nodal points. The novelty of this paper is the use of Voronoi concept in determining the weight functions used in the formulation of the MLS type shape functions.

Keywords: Discrete Least Squares Meshless, crack, Voronoi tessellation, concave boundaries, Steady-state heat conduction.

1 Introduction

Meshless methods have been widely used for solving the practical engineering problems in recent years. These methods do not implement element or any predefined connectivity between nodal points to perform the analysis. They use instead a set of scattered nodal points for both approximating of the unknown function and for discretizing the continuous governing partial differential equations or just for the approximating step. Due to this characteristic, most of the researchers have been interested in implementing meshless methods rather than the well-known Finite Element Method(FEM) or Boundary Element Method(BEM) particularly for solving the problems involving large deformations, moving boundaries or irregular complex geometries.

On the other hand, because that in meshless methods, in contrast to the FEM, the support or influence domains of the sampling points(integration points) have generally overlapping(the shape functions in meshless methods are not restricted to have the Kronecker delta property), these methods yield more accurate results in problems governed with second or higher order derivatives of the unknown function. These types of problems such as heat transfer or fluid dynamics require a high degree of continuity for the unknown function to achieve desirable results. In other words, in meshless methods, with respect to FEM, the shape functions have wider influence domains and have more smoothness.

Those more famous meshless methods implemented for heat transfer simulation until today are Smoothed Particle Hydrodynamic(SPH) method[1–2], Diffuse Approximation Meshless(DAM) method[3], Element Free Galerkin(EFG) method[4–5], Meshless Weighted Least Squares(MWLS) method[6], Reproducing Kernel Particle Method(RKPM)[7], and Meshless Local Petrov-Galerkin(MLPG) method[8–10].

SPH method is a computational method used for

* Corresponding author. E-mail: labibadeh_m@scu.ac.ir

simulating fluid flows. It is a Lagrangian meshless method(where the coordinates move with fluid) and the accuracy of the method can easily be adjusted with respect to variables such as density. Because that heat transfer generally involves complex fluid dynamics, CLEARY and MONAGHAN[11] used the advantages of Lagrangian methods like SPH for solving such problems. They employed a simple alteration to the standard SPH method to ensure continuity in simulating of heat flux across discontinuities in material properties. These researchers implemented a technique in the framework of SPH for improving the accuracy of this method in estimating the second derivatives of the governing heat conduction equations which are involved in an unsteady heat conduction problem. CHEN, et al[12], applied an alternative approach for overcoming the deficiencies of the SPH in solving the unsteady heat conduction problem at the boundaries of a domain where the particles become disordered. They combined the kernel estimate with the Taylor series expansion to develop a Corrective Smoothed Particle Method(CSPM). They declared that with their method, the accuracy of the solution was enhanced not only near and on the boundaries but also within the domain.

DAM may be considered as a generalization of the widely used FEM. It removes some of the limitations of the FEM like the regularity and smoothness of approximated functions in the domain and mesh generating requirements. SADAT and COUTURIER[13] worked on the performance and accuracy of DAM method and used the advantages of this method with respect to the FEM for solving the laminar natural convection problem. Also, SADAT, et al[14], solved a 2D heterogeneous heat conduction problem with this meshless method. SOPHY, et al[15], formulated a meshless approach for simulating the 3D laminar natural heat convection. Sadat and his co-workers reported that DAM can be used in complex geometries and this method is stable and accurate even at high Rayleigh numbers.

In the EFG method, description of the geometry and numerical model of the problem consists only of a set of nodes and a description of exterior boundaries and interior boundaries from any cracks. This method uses moving least-squares interpolants to construct the trial and test functions for the variational principle(weak form). In moving least-square interpolants, the dependent variable at any point is obtained by minimizing a function in terms of the nodal values of the dependent variable in the domain of influence of the point. By implementing this approach, the dependent variable and its derivatives are obtained continuous in the entire domain. Certain key differences are introduced in this method to increase its accuracy; rate of convergence in the vicinity of the steep localized gradients in comparison to DAM. Singh et al employed the EFG method for solving a number of problems in the field of heat transfer such as the 2D fins[16], 3D steady-state heat conduction[17], 3D transient heat conduction[18], the temperature-dependent thermal conductivity problems[19] and finally composite heat transfer[20]. They utilized moving least squares(MLS) approximants to approximate the unknown function of temperature. These MLS approximants were constructed by using a weight function, a basis function and a set of non-constants coefficients. Variational method was used for the discretization of the governing equations. The essential boundary conditions were enforced using the Lagrange multiplier technique.

MWLS method is a pure meshless method which combines the moving least squares approximation scheme and least squares discretization. YAN, et al[21], studied the steady state of heat conduction problems employing MWLS method. LIU, et al[22], extended MWLS method to solve the unsteady-state heat conduction equation and discussed the optimal choice of computational parameters. They reported that MWLS method is much faster than the EFG method, while the accuracy of MWLS is close to or even better than EFG method.

RKPM is similar to the SPH method with one major difference: the development of a correction function for boundary effects. With this correction function, the tensile instability of the SPH has been completely eliminated in RKPM. Recently, CHENG and LIEW[23] used RKPM method for analyzing the 3D transient heat conduction problems. These researchers concluded in their research that RKPM can be used for non-regular geometries and this is an advantage with respect to FEM. They also declared that RKPM yields accurate results in steady-state heat conduction problem and can be extended for un-steady heat conduction.

MLPG is a truly meshless method similar to the MWLS which needs no shadow elements to evaluate the domain integrals like the DAM, EFG or RKPM because that this method is based on local weak-form formulation. However, this method is based on point collocation and is very sensitive to the choice of collocation points. SLADEK, et al[24–26], used MLPG for solving the heat conduction differential equations in non-homogeneous anisotropic mediums. They reported that the limitation of conventional boundary element approaches to non- homogeneous solids is removed by using MLPG method. In another work, MLPG method was employed by QIAN, et al[27] to investigate the 3D transient heat conduction problem in a functionally graded thick plate. HONG and QUAN[28] applied MLPG method to study the steady-state heat conduction problems with irregular complex domains in a 2D space and compared the results with the Finite Volume Method(FVM).

None of the above mentioned approaches simulate heat transfer in domains contain crack or highly irregular concave boundaries. Furthermore, all these approaches except of the MLPG and MWLS methods use at least a background mesh for carrying out the numerical integration which involved in the analysis when the weak form of the governing equations are present in the formulations. Hence, they have not a noticeable advantage over the mesh

dependent approaches like FEM or BEM for using in this study. Although the MPLG is a true meshless method which does not implement any kind of mesh in the analysis, the accuracy of this method as it was mentioned above is very sensitive to the choice of collocation points. Therefore, in this study, based on the advantages of MWLS in simulating the heat conduction phenomenon, it was decided to implement DLSM method which has not been tested against the heat conduction problems yet, and is very similar to the MWLS, and modify it to make it possible to simulate heat conduction in irregular domains containing crack or concave boundaries.

2 DLSM Method

In DLSM which is a true meshless method, the domain of interest is discretized with a set of scattered nodal points and then it is trying to make a squared residual function to be minimized. This function is defined as the summation of the squared residuals of the governing differential equations and its accompanied boundary conditions at the nodal points. Generally in DLSM, the main unknowns(the temperatures at the nodal points in this study) are approximated using the Moving Least Squares(MLS) shape functions. Because the MLS shape functions do not satisfy the Kronecker delta requirement, the boundary conditions are imposed to the model using a penalty approach.

DLSM has been implemented in recent years to solve many engineering problems such as Poisson's equation[29], elliptical partial differential equations[30], transient and steady-state fluid flows[31–32], planar elasticity problems [33–34], error estimate and adaptive refinement for elasticity problems[35–36]. However, none of them can solve such equations on practical irregular domains with concave boundaries or cracks. This is due to the fact that the standard DLSM method like to the other meshless methods fails in determining the support domain of the sampling points in the vicinity of the concave boundaries or cracks accurately and consequently cannot construct their shape functions precisely. In other words, DLSM cannot distinguish the discontinuities between adjacent nodes near or on crack faces or concave boundaries and perhaps the nodes are located in two opposite sides of a concave boundary or crack are incorporated incorrectly in a same support domain. This means that portions of the mentioned crack or opening are considered wrongly as a continuous medium. Some techniques have been implemented in recent years such as visibility, diffraction and transparency[37–38] in meshless methods to overcome such deficiency but each of them has own specific shortcomings and does not possess a general application. These methods are briefly discussed in section 3.3. Hence, in current study, this method has been modified and improved its capacity to conquer such defects using the advantages of the Voronoi tessellation algorithm in constructing the MLS shape functions. This method does not show the shortcomings of the mentioned techniques. It guarantees the continuity and smoothness requirements for the shape functions everywhere around the crack tip and at the same time does not extend the time of processing.

It is worth to mention here again before further continue that in this study the main task is to modify the standard DLSM method to make possible that the steady-state heat conduction problem can be solved in domains contain complex geometry with concave boundaries or crack. Standard DLSM cannot solve such problems and obtained results using this method are meaningless. So, it is not intended and basically it is not possible to compare the results obtained from VDLSM with the standard DLSM. Furthermore, FEM has been used in this study just for verifying the results obtained from VDLSM where analytical solutions are not available. By using VDLSM, the predefined nodal connectivity which is an essential need in FEM is not required and the discontinuity between temperatures at the element borders which may be observed in FEM does not occur in VDLSM because of the smoothness nature of MLS shape functions.

This paper is organized as follows. Section 3 introduces the MLS approximation in conjunction with Voronoi tessellation approach used for shape function construction. In section 4, VDLSM method for solving heat conduction problems is formulated. Four benchmark numerical examples are solved in section 5. Finally, some useful conclusions are summarized in section 6.

3 VDLSM Method

In the present study, as mentioned before, the advantage of Voronoi tessellation used for constructing MLS shape functions. Creation of these shape functions consists of four stages as below.

3.1 Support domain formation

In previous works on DLSM method, two general methods have been used: In the first method, the radius of the support domain has been considered as a constant value. So, the nodes which lie within a circle around a node *j*(the center of the circle) are involved in the shape function construction for node *j*. This method is easy to implement but it can only be efficiently used for regular nodal configurations. In order to overcome this deficiency, the average of the distances of the *n* closest points to node *i* multiplied by a constant number was used for obtaining the support domain radius of node *j*. Using this method leads to give accurate results for geometrically regular domains with irregular nodal arrangements. However, this method is not easily applicable on a domain which includes cracks or concave boundaries(irregular domains), the main challenge of this work. Thus, in this study in addition to propose DLSM method for heat conduction analysis, a more flexible and effective method is proposed to overcome aforementioned deficiency.

In this method the support domain of node i includes only of the neighbor nodes of node j. Neighbor nodes of node j are detected using Voronoi diagram algorithm. In this way, each node has a Voronoi cell. A Voronoi cell of node j is defined as the collection of the points x that are located closer to node j than any other nodes likes node i (see Fig. 1)[39].

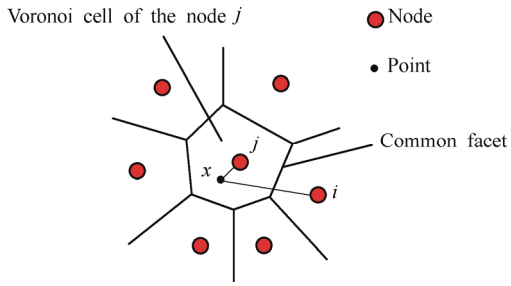

Fig. 1. Voronoi diagram and neighbor nodes of node j

In the mathematical formulation this definition can be stated as follows:

$$V_j = \left\{ x \in \Re^n, d(x,\xi_j) < d(x,\xi_i) \text{ for } i \neq j \right\}, \tag{1}$$

where V_j is the Voronoi cell of node j, and d is the Euclidean distance between point x and node $\xi_i \in \Re^n$ defined as

$$d(x,\xi_i) = \|x-\xi_i\| = \sqrt{(x_1-\xi_{i1})^2+(x_2-\xi_{i2})^2+(x_3-\xi_{i3})^2}\,. \tag{2}$$

Once the Voronoi cells are created, the nodes which have a common facet with the Voronoi cell of node j are considered as the first layer of neighbor nodes(Fig. 1). We can define more than one layer of neighbor nodes if needed.

3.2 Basis functions

The second step to construct MLS shape functions is the approximation of the function defined as

$$\boldsymbol{T}(x) = \sum_{i=1}^{r} p_i(x)a_i(x) = \boldsymbol{P}^{\mathrm{T}}(x)\boldsymbol{a}(x), \tag{3}$$

$$\boldsymbol{P}^{\mathrm{T}}(x) = [1, x, y, x^2, xy, y^2, \cdots, x^m, x^{(m-1)}y, \cdots, xy^{(m-1)}, y^m], \tag{4}$$

where $\boldsymbol{a}(x)$ is the vector of coefficients and $\boldsymbol{P}(x)$ is the vector of basis functions; m is the order of basis functions and r is the total number of the basis function terms. In the proposed method, the number of the layers of the neighbor nodes is considered to be equal to the order of the basis functions. In other words, the value of m determines the number of neighbor layers used for constructing the support domain. For example, in Fig. 2, two layers of neighbor nodes are selected for creating a second order basis functions. This method guarantees the required number of the nodes for basis functions calculation and there is no need to additional methods to determine the number of the nodes for the support domain. In this paper, the basis functions of the form $\boldsymbol{P}(x) = [1, x, y, x^2, xy, y^2]$ (m=2 and r=6) was used, means that two layers of the neighbor nodal points have been employed.

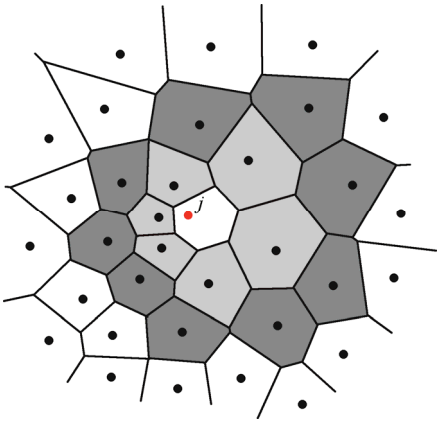

Fig. 2. Forming support domain by two layers of neighbors

3.3 Definition of the weight function for non-convex domains

In this work, a cubic spline weight function(Eq. (5)) was considered. Accurate solution of non-convex boundary problems or cracked domains requires the construction of smooth continuous weight functions near crack. This cubic spline function produces smooth continuous and differentiable results with relatively coarse scattered nodal points[40].

$$W_j(x) = w(\bar{d}) = \begin{cases} \left\langle \dfrac{2}{3} - 4\bar{d}^2 + 4\bar{d}^3 \,\middle|\, \text{for } |\bar{d} \leqslant \dfrac{1}{2} \right\rangle, \\ \left\langle \dfrac{4}{3} - 4\bar{d} + 4\bar{d}^2 - \dfrac{4}{3}\bar{d}^3 \,\middle|\, \text{for } \left|\dfrac{1}{2} < \bar{d} \leqslant 1 \right\rangle, \\ \langle 0 \,|\, \text{for } |\bar{d} > 1 \rangle. \end{cases} \tag{5}$$

Where $\bar{d} = d_i / d_{wj}$, $d_i = \|\boldsymbol{x}_i - \boldsymbol{x}_j\|$ and d_{wj} is the radius of the weight function of point j. d_{wj} is set to be the d_i of the farthest node located in the support domain of node j multiplied by a constant number which is considered in this study as 1.1. Some considerations should be taken into account for computing d_i in this study.

It should be recalled that by Voronoi approach used here, the nodes which are located in the support domain of node j are not determined based on their straight distances from node j. In other words, if the distance of a node i to node j is smaller than the distance between nodes j and k, node i is not necessarily considered in the support domain of node j. For example, for the case m=1, node i in Fig. 3 does not

place in the *j*'s support domain even if it's distance from node *j* is smaller than the distance of the node m from node *j*. Because that node *i* in that Fig. has no common facet with *j*'s Voronoi cell. Furthermore, note that the node k which is located behind the crack vertex is excluded from the support domain of node *j* even if it is located at a very close position to node *j*, because the vertex which located on the crack line is not considered as the common facet.

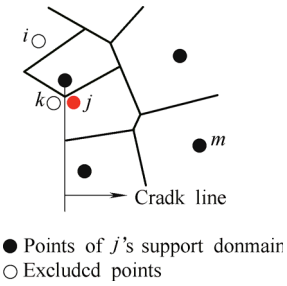

Fig. 3. Nodes excluded from the support domain

By this approach, for the case m=1(one layer of neighbor's Voronoi cells is considered), d_i can be normally defined as the straight distance of node *i* from node *j* and no additional operation is needed. However, for the case $m \geqslant 2$(two layers of neighbor's Voronoi cells are considered), the distance d_i cannot be measured along a straight line connects nodes *i* and *j* because this line may pass through a cell which is not a neighbor cell of node *j*. This problem can be fixed by imposing a constraint. This constraint is that for computing d_i , at first a path must be defined between nodes *i* and *j*.

This path which connects node *i* to node *j* must always passes through the neighbor cells of node *j*. By this way, for computing d_i in Fig. 4, the path which connects two nodes *i* and *j* passes from a middle node k. according to this Fig. d_i is the summation of P_1 and P_2:

$$d_i = P_1 + P_2, \tag{6}$$

$$P_1 = \|x_k - x_j\|, P_2 = \|x_k - x_i\|. \tag{7}$$

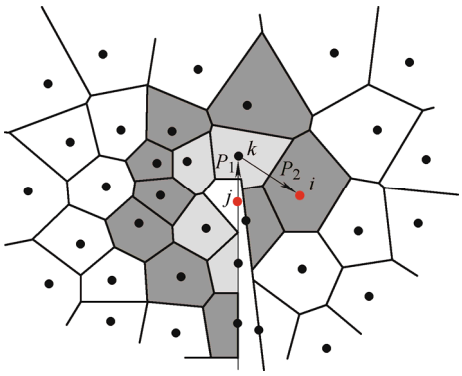

Fig. 4. Support domain for m=2 in a cracked domain

Before further continuing of the formulation, as mentioned in introduction and for better understanding the scheme which was described above, let us review briefly some techniques which have been implemented by researchers in recent years to incorporate the effects of the discontinuities like cracks into the analysis. These techniques may not be understood well by the readers before this stage of the study.

In visibility technique, the weight of node X_I at point X is set to zero if the segment that joins them is cut by a crack. Hence, by this way, the weight function and subsequently the shape functions at point X are modified considering the discontinuity opaque for rays of light coming from the node X_I (see Fig.5)[37]. In other words, by this approach, a discontinuity is distinguished as a part of a medium which light cannot travel through it. With this method, the concave boundaries are detected but the continuity condition of the weight and obtained shape functions is violated near the crack tip (yields spurious discontinuity) because that at the crack tip, an artificial discontinuity inside the domain is constructed as shown in Fig. 5[41].

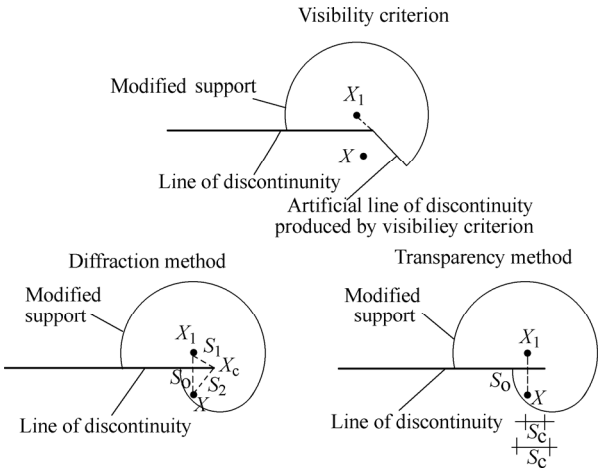

Fig. 5. Visibility Criterion, diffraction, and transparency techniques[37]

In diffraction method, if the segment that joins node X_I to point X is cut by a crack, the normalized distance $\bar{d}$ which it was used in Eq. (5) in this study, is defined according to the length of the shortest path from node X_I to point X passing by the point of the crack tip X_C: $X_I - X - X_C$. In mathematical form this can be written as

$$\bar{d} = \frac{\| x - x_c \| + \| x_c - x_i \|}{S_0} = \frac{S_1 + S_2}{S_0} \text{ (see Fig. 5).}$$

The weight function of node X_I is then continuous except across the crack.

By using transparency method, if the segment that joins node X_I to point X is cut by a crack, the normalized distance $\bar{d} = \frac{d_i}{S_0}$ in Eq. (5) is augmented by a transparency function that increases with the distance between the crack tip and the intersection of the segment with the crack. That is

$$\bar{d} = \frac{\| x - x_i \|}{S_0} + f_t(S_c)$$

with $f_t(0)=0$ and f_t a strictly increasing function to choose(see Fig. 5). Transparency criterion gives sharply varying shape functions for the nodes near the crack[41].

From the above reviewing, it is revealed that these techniques are not guaranteeing the smoothness of the shape functions near the crack or crack tip and also are not straight-forward schemes. This is due to the fact that these methods do not construct support domain of the nodal points considering the effect of crack or other discontinuity from the first step of the analysis procedure and they are trying to modify the weight and shape functions after that the support domains are constructed. However, by the proposed method in this study, the aforementioned deficiency is removed completely.

Coming back to the main discussion, the weight function derivatives are computed using the chain role:

$$\frac{\partial W}{\partial x}=\frac{\partial W}{\partial \bar{d}}\frac{\partial \bar{d}}{\partial x},\ \text{and}\ \ \frac{\partial W}{\partial y}=\frac{\partial w}{\partial \bar{d}}\frac{\partial \bar{d}}{\partial y}. \tag{8}$$

Furthermore, because that VDLSM method is a method which works with the strong form of the governing equations, so the second derivatives should be calculated for heat conduction problems:

$$\begin{aligned}\frac{\partial^2 W}{\partial x^2}&=\frac{\partial^2 w}{\partial \bar{d}^2}\left(\frac{\partial \bar{d}}{\partial x}\right)^2+\frac{\partial w}{\partial \bar{d}}\left(\frac{\partial^2 \bar{d}}{\partial x^2}\right),\\ \frac{\partial^2 W}{\partial x\partial y}&=\left(\frac{\partial^2 w}{\partial \bar{d}^2}\right)\frac{\partial \bar{d}}{\partial x}\frac{\partial \bar{d}}{\partial y}+\frac{\partial w}{\partial \bar{d}}\left(\frac{\partial^2 \bar{d}}{\partial x\partial y}\right),\\ \frac{\partial^2 W}{\partial y^2}&=\frac{\partial^2 w}{\partial \bar{d}^2}\left(\frac{\partial \bar{d}}{\partial y}\right)^2+\frac{\partial w}{\partial \bar{d}}\left(\frac{\partial^2 \bar{d}}{\partial y^2}\right).\end{aligned} \tag{9}$$

According to above equations, derivatives of $\bar{d}$ are needed and must be computed. Since d_{w} is a constant, all that needed are derivatives of d_i. According to Eq. (7), P_1 is not changed. So, only the derivatives of P_2 should be calculated. The first derivatives are

$$\begin{aligned}\frac{\partial P_2}{\partial x}&=\frac{x_i-x_k}{P_2},\\ \frac{\partial P_2}{\partial y}&=\frac{y_i-y_k}{P_2},\end{aligned} \tag{10}$$

and the second derivatives are

$$\begin{aligned}\frac{\partial^2 P_2}{\partial x^2}&=\frac{1}{P_2}-\frac{(x_i-x_k)^2}{P_2^3},\\ \frac{\partial^2 P_2}{\partial y^2}&=\frac{1}{P_2}-\frac{(y_i-y_k)^2}{P_2^3},\\ \frac{\partial^2 P_2}{\partial x\partial y}&=\frac{-(y_i-y_k)(x_i-x_k)}{P_2^3}.\end{aligned} \tag{11}$$

3.3 MLS shape function construction

Weighted discrete *L*2 norm function is defined by

$$J=\sum_{j=1}^{n_s}W_j(x-x_j)(\boldsymbol{P}^{\mathrm{T}}(x_j)a(x_j)-\boldsymbol{T}_j^h)^2, \tag{12}$$

where $\boldsymbol{T}_j^h$ is the approximated unknown function (in this study the temperature) of node j, and n_s is the total number of the nodes in the support domain of sampling point x and W_j is the weight function in node j.

The unknown function; $T(\boldsymbol{x})$; in sampling point x can be obtained by minimizing the function J (Eq. (12)) as follows:

$$\boldsymbol{T}(x)=\boldsymbol{P}^{\mathrm{T}}(x)\boldsymbol{A}^{-1}(x)\boldsymbol{B}(x)\boldsymbol{T}^h, \tag{13}$$

where $\boldsymbol{T}^h$ is a vector collecting the nodal values of temperature as follows:

$$\boldsymbol{T}^h=\begin{bmatrix}T_1^h & T_2^h & \cdots & T_{n_s}^h\end{bmatrix}, \tag{14}$$

and $A(x)$ and $B(x)$ are defined as

$$A(x)=\sum_{j=1}^{n_s}W_j(x-x_j)P(x_j)P^{\mathrm{T}}(x_j), \tag{15}$$

$$\begin{aligned}B(x)=\big[&W_1(x-x_j)P(x_1),W_2(x-x_2)P(x_2),\cdots,\\ &W_{n_s}(x-x_{n_s})P(x_{n_s})\big],\end{aligned} \tag{16}$$

Eq. (13) is rewritten in the following form:

$$\boldsymbol{T}(x)=\boldsymbol{N}^{\mathrm{T}}(x)\boldsymbol{T}^h, \tag{17}$$

where $\boldsymbol{N}^{\mathrm{T}}(x)=\boldsymbol{P}^{\mathrm{T}}(x)\boldsymbol{A}^{-1}(x)\boldsymbol{B}(x)$ is transpose of the vectors of MLS shape functions. The seobtained shape functions can be appliedreadily to model the temperature field around and near the cracktip without need to use special modifications as it is required in techniques such as visibility, diffraction or transparency methods[41].

In the solution of partial differential equations, it is often necessary to obtain the shape function derivatives. The first order derivatives of the MLS shape function can be obtained as follows:

$$\begin{aligned}\frac{\mathrm{d}\boldsymbol{N}}{\mathrm{d}x}&=\frac{\mathrm{d}\boldsymbol{P}^{\mathrm{T}}}{\mathrm{d}x}\boldsymbol{A}^{-1}\boldsymbol{B}+\boldsymbol{P}^{\mathrm{T}}\frac{\mathrm{d}\boldsymbol{A}^{-1}}{\mathrm{d}x}\boldsymbol{B}+\boldsymbol{P}^{\mathrm{T}}\boldsymbol{A}^{-1}\frac{\mathrm{d}\boldsymbol{B}}{\mathrm{d}x},\\ \frac{\mathrm{d}\boldsymbol{N}}{\mathrm{d}y}&=\frac{\mathrm{d}\boldsymbol{P}^{\mathrm{T}}}{\mathrm{d}y}\boldsymbol{A}^{-1}\boldsymbol{B}+\boldsymbol{P}^{\mathrm{T}}\frac{\mathrm{d}\boldsymbol{A}^{-1}}{\mathrm{d}y}\boldsymbol{B}+\boldsymbol{P}^{\mathrm{T}}\boldsymbol{A}^{-1}\frac{\mathrm{d}\boldsymbol{B}}{\mathrm{d}y}.\end{aligned} \tag{18}$$

While the second order derivatives of MLS shape functions, which are only required when the second order derivatives are present in the governing differential equations, like present case, are obtained as follows:

$$\frac{\mathrm{d}^2\boldsymbol{N}}{\mathrm{d}x^2}=\frac{\mathrm{d}^2\boldsymbol{p}^{\mathrm{T}}}{\mathrm{d}x^2}\boldsymbol{A}^{-1}\boldsymbol{B}+\boldsymbol{p}^{\mathrm{T}}\frac{\mathrm{d}^2\boldsymbol{A}^{-1}}{\mathrm{d}x^2}\boldsymbol{B}+\boldsymbol{p}^{\mathrm{T}}\boldsymbol{A}^{-1}\frac{\mathrm{d}^2\boldsymbol{B}}{\mathrm{d}x^2}+2\left(\frac{\mathrm{d}\boldsymbol{p}^{\mathrm{T}}}{\mathrm{d}x}\frac{\mathrm{d}\boldsymbol{A}^{-1}}{\mathrm{d}x}\boldsymbol{B}+\frac{\mathrm{d}\boldsymbol{p}^{\mathrm{T}}}{\mathrm{d}x}\boldsymbol{A}^{-1}\frac{\mathrm{d}\boldsymbol{B}}{\mathrm{d}x}+\boldsymbol{p}^{\mathrm{T}}\frac{\mathrm{d}\boldsymbol{A}^{-1}}{\mathrm{d}x}\frac{\mathrm{d}\boldsymbol{B}}{\mathrm{d}x}\right),$$

$$\frac{\mathrm{d}^2\boldsymbol{N}}{\mathrm{d}y^2}=\frac{\mathrm{d}^2\boldsymbol{p}^{\mathrm{T}}}{\mathrm{d}y^2}\boldsymbol{A}^{-1}\boldsymbol{B}+\boldsymbol{p}^{\mathrm{T}}\frac{\mathrm{d}^2\boldsymbol{A}^{-1}}{\mathrm{d}y^2}\boldsymbol{B}+\boldsymbol{p}^{\mathrm{T}}\boldsymbol{A}^{-1}\frac{\mathrm{d}^2\boldsymbol{B}}{\mathrm{d}y^2}+2\left(\frac{\mathrm{d}\boldsymbol{p}^{\mathrm{T}}}{\mathrm{d}y}\frac{\mathrm{d}\boldsymbol{A}^{-1}}{\mathrm{d}y}\boldsymbol{B}+\frac{\mathrm{d}\boldsymbol{p}^{\mathrm{T}}}{\mathrm{d}y}\boldsymbol{A}^{-1}\frac{\mathrm{d}\boldsymbol{B}}{\mathrm{d}y}+\boldsymbol{p}^{\mathrm{T}}\frac{\mathrm{d}\boldsymbol{A}^{-1}}{\mathrm{d}y}\frac{\mathrm{d}\boldsymbol{B}}{\mathrm{d}y}\right),$$

$$\frac{\mathrm{d}^2\boldsymbol{N}}{\mathrm{d}xy}=\frac{\mathrm{d}^2\boldsymbol{p}^{\mathrm{T}}}{\mathrm{d}xy}\boldsymbol{A}^{-1}\boldsymbol{B}+\boldsymbol{p}^{\mathrm{T}}\frac{\mathrm{d}^2\boldsymbol{A}^{-1}}{\mathrm{d}xy}\boldsymbol{B}+\boldsymbol{p}^{\mathrm{T}}\boldsymbol{A}^{-1}\frac{\mathrm{d}^2\boldsymbol{B}}{\mathrm{d}xy}+\frac{\mathrm{d}\boldsymbol{p}^{\mathrm{T}}}{\mathrm{d}x}\frac{\mathrm{d}\boldsymbol{A}^{-1}}{\mathrm{d}y}\boldsymbol{B}+\frac{\mathrm{d}\boldsymbol{p}^{\mathrm{T}}}{\mathrm{d}x}\boldsymbol{A}^{-1}\frac{\mathrm{d}\boldsymbol{B}}{\mathrm{d}y}+\frac{\mathrm{d}\boldsymbol{p}^{\mathrm{T}}}{\mathrm{d}y}\frac{\mathrm{d}\boldsymbol{A}^{-1}}{\mathrm{d}x}\boldsymbol{B}+\boldsymbol{p}^{\mathrm{T}}\frac{\mathrm{d}\boldsymbol{A}^{-1}}{\mathrm{d}x}\frac{\mathrm{d}\boldsymbol{B}}{\mathrm{d}y}+\frac{\mathrm{d}\boldsymbol{p}^{\mathrm{T}}}{\mathrm{d}y}\boldsymbol{A}^{-1}\frac{\mathrm{d}\boldsymbol{B}}{\mathrm{d}x}+\boldsymbol{p}^{\mathrm{T}}\frac{\mathrm{d}\boldsymbol{A}^{-1}}{\mathrm{d}y}\frac{\mathrm{d}\boldsymbol{B}}{\mathrm{d}x}. \tag{19}$$

4 VDLSM Formulation for Steady-State Heat Conduction Phenomenon

In this section, to demonstrate the efficiency of the VDLSM, it is formulated for solving the steady-state heat conduction problems. Considering the following steady-state temperature distribution equation:

$$k\nabla^2 T(x)+\rho Q=0 \text{ in } \Omega, \tag{20}$$

where k and ρ are the thermal conductivity and mass density, respectively; Q is the heat source per unit mass; Ω is the domain of the problem and $x=[x \quad y]^{\mathrm{T}}$ the Cartesian coordinates. The equation is subjected to the following boundary conditions:

$$T=\overline{T} \text{ on } \Gamma_{b1}, \tag{21}$$

$$n\bullet k\nabla T=\overline{q}=0 \text{ on } \Gamma_{b2}, \tag{22}$$

$$n\bullet k\nabla T=h(T_a-T) \text{ on } \Gamma_{b3}, \tag{23}$$

where $\overline{T}$ and $\overline{q}$ are the prescribed temperature and heat flux on Γ_{b1} and Γ_{b2} boundaries, respectively. T_a is a prescribed ambient temperature on Γ_{b3} and n represents the unit outward normal to the boundary and h is the convection heat transfer coefficient.

Eq. (20) can now be rewritten in the residual form as

$$R_{\Omega}=\sum_{n=1}^{n_d}\left(L(T)+f\right) \text{ in } \Omega, \tag{24}$$

where n_d is the total number of the nodes used to discretize the problem domain Ω and $L(\ )$ is a second order differential operator defined as

$$L(\ )=L_{xx}(\ )+L_{yy}(\ ), \tag{25}$$

where L_{xx} and L_{yy} for the steady-state heat conduction equation are defined as

$$L_x x=k\frac{\partial^2(\ )}{\partial x^2}, L_{yy}=\frac{\partial^2(\ )}{\partial y^2}, \tag{26}$$

and f is defined as

$$f=\rho Q. \tag{27}$$

The boundary conditions i.e. Eqs. (21) to (23) can also be rewritten in the residual forms as

$$R_{\Gamma_{b1}}=\sum_{n=1}^{n_{b1}}(T_n-\overline{T}) \text{ on } \Gamma_{b1}, \tag{28}$$

$$R_{\Gamma_{b2}}=\sum_{n=1}^{n_{b2}}(L'(\boldsymbol{T}_n)-\overline{\boldsymbol{q}}) \text{ on } \Gamma_{b2}, \tag{29}$$

$$R_{\Gamma_{b3}}=\sum_{n=1}^{n_{b3}}\left[L'(\boldsymbol{T}_n)-h(\boldsymbol{T}_a-\boldsymbol{T}_n)\right] \text{ on } \Gamma_{b3}, \tag{30}$$

where n_{b1}, n_{b2} and n_{b3} are the total number of the nodes on Γ_{b1}, Γ_{b2} and Γ_{b3} boundaries, respectively and L' is a first order differential operator defined as below:

$$L'(\ )=L'_x(\ )+L'_y(\ ) \text{ on } \Gamma_{b2} \text{ and } \Gamma_{b3}, \tag{31}$$

where $L'_x=n_x\bullet k\frac{\partial(\ )}{\partial x}$ and $L'_y=n_y\bullet k\frac{\partial(\ )}{\partial x}$.

Now a functional using the penalty approach for imposing the boundary conditions is defined as

$$I=\sum_{n=1}^{nd}\left[\boldsymbol{L}(\boldsymbol{T}_n)+f\right]^2+\sum_{n=1}^{nb_1}\alpha_1\left[\boldsymbol{T}_n-\overline{\boldsymbol{T}}\right]^2+\sum_{n=1}^{nb_2}\alpha_2\left[L'(\boldsymbol{T}_n)-\overline{\boldsymbol{q}}\right]^2+\sum_{n=1}^{nb_3}\alpha_3\left[L'(\boldsymbol{T}_n)-h(\boldsymbol{T}_a-\boldsymbol{T}_n)\right]^2, \tag{32}$$

where α_1, α_2 and α_3 are the penalty coefficients for Γ_{b1}, Γ_{b2} and Γ_{b3} boundaries, respectively.

Minimization of this functional with respect to the nodal variables; i.e. the temperatures of the nodes $(T_i, i=$

$1, 2, \cdots, n_d$) where n_d is defined as the total number of the nodal points leads to the following system of equations:

$$\boldsymbol{KT} = \boldsymbol{F}, \tag{33}$$

where $\boldsymbol{T} = [T_1, T_2, \cdots, T_{nd}]^{\mathrm{T}}$ is a vector collecting the unknown scalar nodal temperatures and $\boldsymbol{K}$ and $\boldsymbol{F}$ are the coefficient matrix and right hand side known vector respectively with typical components defined as follows:

$$K_{ij} = \sum_{n=1}^{nd} \left[L(N_i)\right]_n^{\mathrm{T}} \left[L(N_j)\right]_n + \alpha_1 \sum_{n=1}^{nb_1} \left[N_i\right]_n^{\mathrm{T}} \left[N_j\right]_n + \alpha_2 \sum_{n=1}^{nb_2} \left[L'(N_i)\right]_n^{\mathrm{T}} \left[L'(N_j)\right]_n + \alpha_3 \sum_{n=1}^{nb_3} \left[L'(N_i) + h(N_i)\right]_n^{\mathrm{T}} \left[L'(N_j) + h(N_j)\right]_n, \tag{34}$$

$$F_i = \sum_{n=1}^{nd} \left[L(N_i)\right]_n^{\mathrm{T}} f_n + \alpha_1 \sum_{n=1}^{nb_1} \left[N_i\right]_n^{\mathrm{T}} \bar{T}_n + \alpha_2 \sum_{n=1}^{nb_2} \left[L'(N_i)\right]_n^{\mathrm{T}} \bar{q}_n - \alpha_3 \sum_{n=1}^{nb_3} \left[L'(N_i) + h(N_i)\right]_n^{\mathrm{T}} \left[hT_a\right]_n. \tag{35}$$

The coefficient matrix $\boldsymbol{K}$ is seen to be a square matrix with a dimension $nd \times nd$, where, nd is the total number of the nodes used to discretize the problem domain. Furthermore, $\boldsymbol{K}$ is a symmetric and positive-definite matrix, irrespective to the characteristics of the differential operators L and L'. Furthermore, using the Voronoi based MLS shape functions makes K to be banded due to a few numbers of nodes which are included in a support domain. Therefore, the final system of equations can be solved via efficient iterative solvers if required.

5 Numerical Examples

In this part, the efficiency of the recommended VDLSM method in the solution of the steady-state heat conduction problems is investigated via solving four benchmark examples. The obtained results are compared with the exact analytical or approximate numerical results obtained from FEM using ABAQUS standard software.

5.1 Steady-state heat conduction in a rectangular domain

As a first example, an ordinary problem; a rectangular domain; with the dimensions of 1 m×0.8 m(see Fig. 6), was chosen. The thermal conductivity is 1.2 W/(m℃). Upper boundary is subjected to an inflow heat flux $\bar{q}$ = 500 W/m^2; other boundaries are maintained at a constant temperature 0 ℃. No heat source exists in the domain.

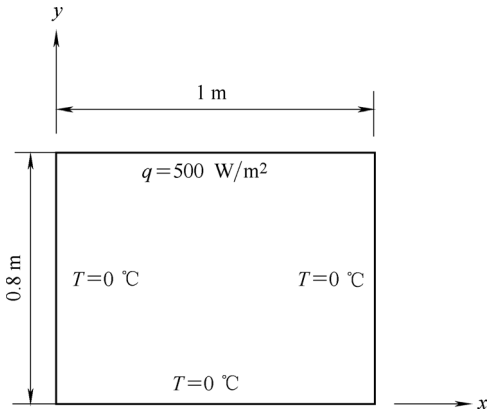

Fig. 6. Geometry and boundary condition for first example

The exact analytical solution obtained from BUDAK et al[42] is brought here as follows:

$$T(x,y) = \frac{4\bar{q}a}{k\pi^2} \sum_{m=0}^{\infty} \frac{\sinh\left\{\left[\frac{(2m+1)\pi}{a}\right] y\right\} \sin\left\{\left[\frac{(2m+1)\pi}{a}\right] x\right\}}{\cosh\left\{\left[\frac{(2m+1)\pi}{a}\right] b\right\} (2m+1)^2}. \tag{36}$$

The problem was solved with three different regular nodal arrangements containing 357, 1353 and 3651 nodal points respectively in order to investigate the convergence rate of this method. Fig. 7 compares the temperature contours obtained from VDLSM method with the corresponding results obtained from the exact solution. Also, for making a possibility to compare the obtained results from VDLSM with other meshless methods, the results obtained from EFG and MWLS for this particular example have been shown in Fig. 7.

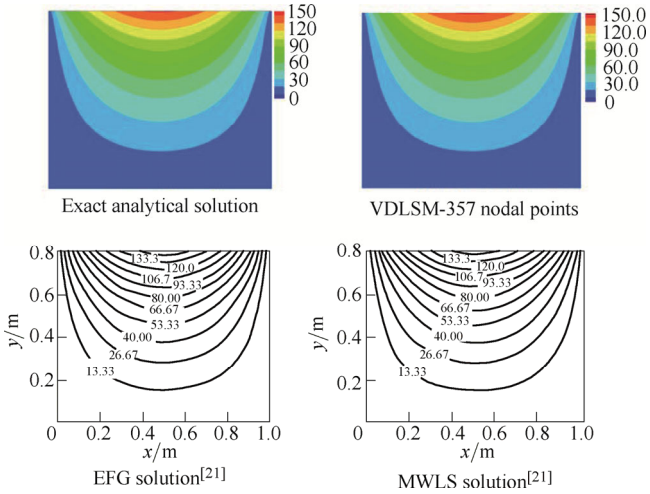

Fig. 7. Contours of Temperature (℃)

It can be seen that VDLSM shows more agreement with analytical results than these methods. Temperature distribution along the upper boundary is depicted in Fig. 8. Fig. 9 shows the comparison of different results along a vertical section at x=0.5.

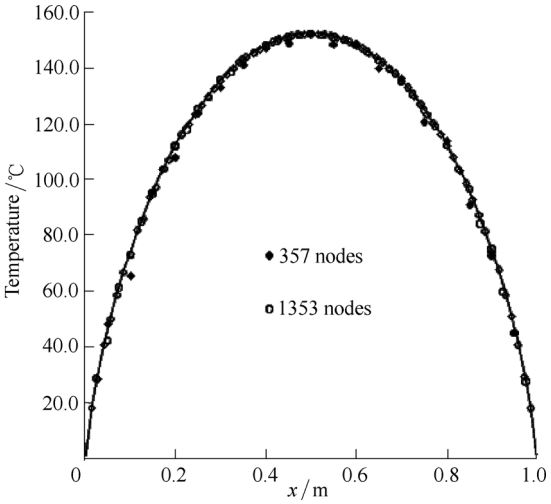

Fig. 8. Temperature distribution on y=0.8(℃)

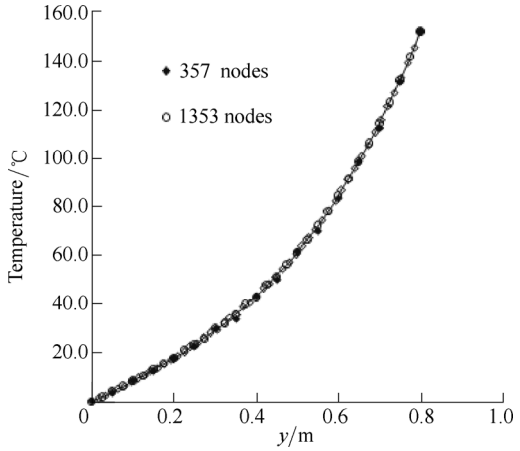

Fig. 9. Temperature on central vertical line (x=0.5)(℃)

From these figures, it can be seen that there is no sensible difference between the obtained results from VDLSM for different number of regular nodal arrangements. This shows that obtained results from VDLSM method for this example are not sensitive to the number of nodes greater than 357.

Hence, it can be said that VDLSM has a good convergence rate and high accuracy in this particular problem similar to MWLS method in their work. It can be seen that there is a good coincidence between the results obtained by VDLSM and exact solution. A $L2$-error has been defined for this example as below:

$$E_{\text{exact}}^{\text{total}} = \left(\frac{\sum_{k=1}^{N} \left[(T_k - \hat{T}_k)^T (T_k - \hat{T}_k) \right]}{N} \right)^{1/2} . \qquad (37)$$

In the above relation, T_k is the approximate temperature and T_k is the exact temperature. N is the total number of nodal points in the domain. Fig. 10 shows such defined L2-error distribution for this example in the domain.

5.2 Insulation of vapor transport in a pipe

As a second example, the vapor transport in a pipe with diameter of 200 mm was considered. The pipe was covered by a thermal insulation layer forming a square shape section of 400 mm length as shown in Fig. 11.

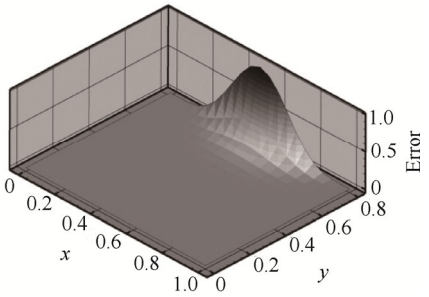

Fig. 10. $L2$-Error distribution for example 5.1

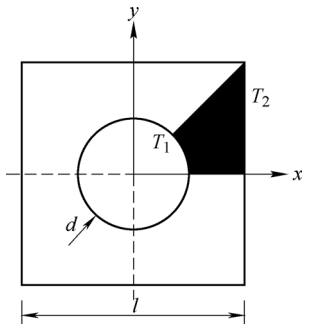

Fig. 11. Vapor transport in a thermal insulated pipe

Inside and outside surface temperatures of the pipe are maintained at the values T_1=200 ℃ and T_2=60 ℃, respectively. The thermal conductivity of the heat insulation layer is considered as 0.1 W/(m℃).

Due to the symmetry, only one eighth sector of the problem domain was modeled.

The problem was solved with 441 regular and 398 irregular nodal point arrangements. The problem was also simulated by FEM based ABAQUS standard software as a reference solution due to the lack of the analytical solution. Fig. 12 shows the nodal configurations of FEM and VDLSM.

Four hundred linear quadrilateral-DS4-elements(a 4-node heat transfer quadrilateral shell) were used from the element library of ABAQUS software for FEM modeling. The temperature contours obtained using the VDLSM with regular and irregular grid and the solution of FEM were compared in Fig. 13.

In Fig. 13, also similar results which obtained by Hong and QUAN from another meshless method i.e. MLPG have been depicted. As it can be seen, the proposed method shows more accurate results than MLPG method. To obtain a more accurate comparison, temperature distributions along two radial lines (bottom and upper boundaries) are demonstrated in Figs. 14 and 15.The comparisons show excellent agreements between the results and confirm the high degree of accuracy of the proposed method. Solving this example also demonstrates that the results obtained from VDLSM are not sensitive to the arrangement of the nodal points (regular or irregular) in contrast to the MLPG method which was mentioned before in literature review.

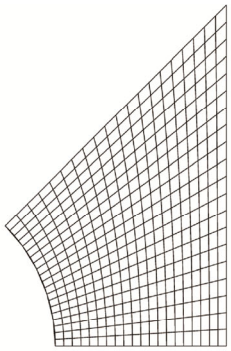

(a) FEM model with 400 linear quadrilateral elements

(b) VDLSM model with 441 regular nodal network

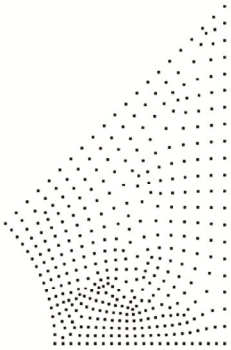

(c) VDLSM model with 398 erregular nodal networks

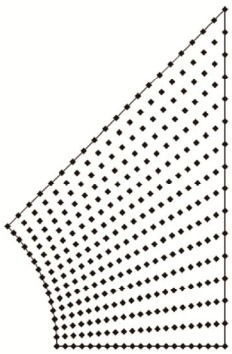

(d) MLPG model wirh 336 regular nodal networks

Fig. 12. FEM and VDLSM models for the second example

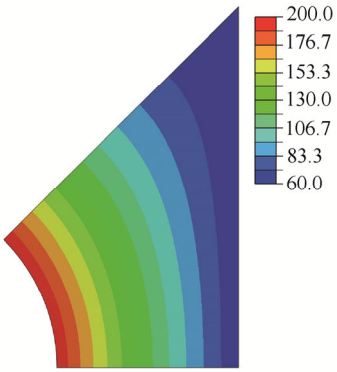

(a)FEM-400 DS4 ABAQUS elements

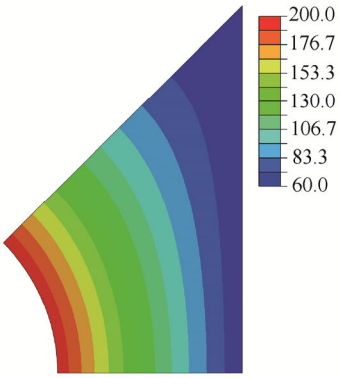

(b) VDLSM-441 regular nodal arrangement

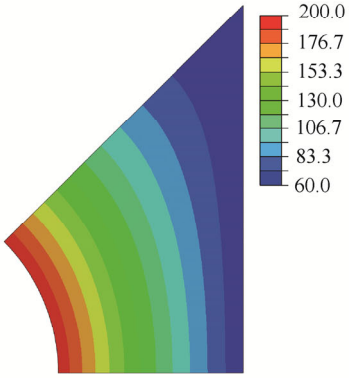

(c) VDLSM-398 irregular nodal arrangement

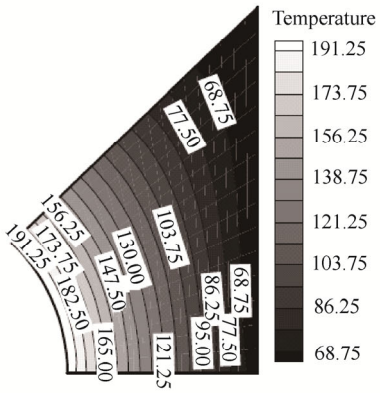

(d) MLPG-336 regular nodal arrangement[28]

Fig. 13. Temperature field around the tube (℃)

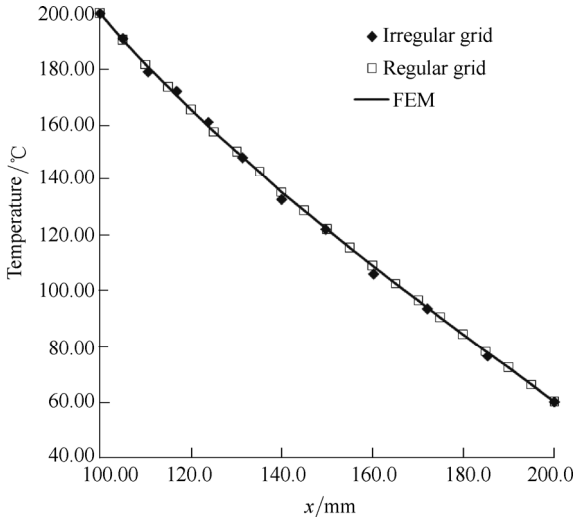

Fig. 14. Temperature distribution along the bottom boundary(y=0) (℃)

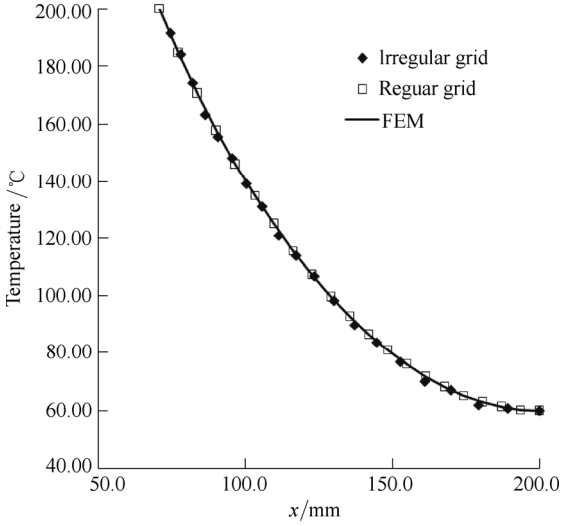

Fig. 15. Comparison of temperature (℃) distribution along the upper boundary (second Example)

5.3 Finite plate with an inclined insulated crack

In order to control the efficiency of the VDLSM method in cracked domains, a square plate containing an inclined insulated crack was considered as the third example.

The top and bottom boundaries are subjected to constant temperatures T_0 and $-T_0$, respectively, where m T_0 is considered as 100 ℃. The other boundaries are adiabatic. The width of the plate is l=100 mm and the length of the crack is a=60 mm. The angle of the crack with the x-axis is set to θ=45° and the center of the crack places on the center of the square plate. The thermal conductivity is considered as $k = 1.2\ W/(\text{m}℃)$. The geometry of the problem and nodal configuration with 2442 nodes are exhibited in Fig. 16 and Fig. 17, respectively.

As shown in Fig. 17, the crack was considered as a longitudinal notch with rounded tips and free flux boundary condition was applied on its faces. Because that the tips of the crack are considered rounded, there is no need for incorporating the singularity of stresses in the analysis.

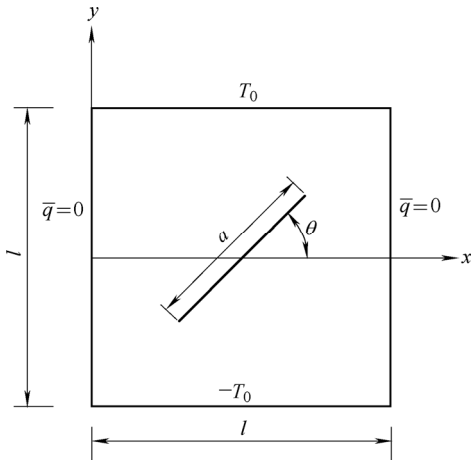

Fig. 16. Geometric configuration of the squared plate with an inclined crack

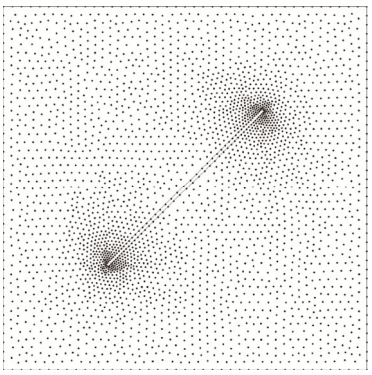

Fig. 17. Irregular nodal configuration of the squared plate with an inclined crack

Results of the FEM solution with 2151 DS4 ABAQUS elements were considered as the exact solution. Fig.18

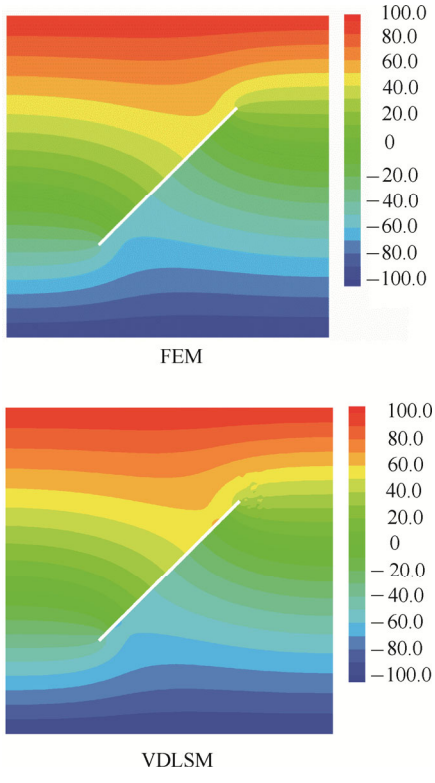

Fig. 18. Comparision of temperature(℃) contours for the squared plate with an inclined crack

comparesthe temperature fields in the domain obtained from FEM and VDLSM. Temperature distributions along the upper side of the crack line and central horizontal line are depicted in Fig. 19. Results show that VDLSM method is capable to predict temperature field in highly complex geometries-cracked domains- with a high accuracy.

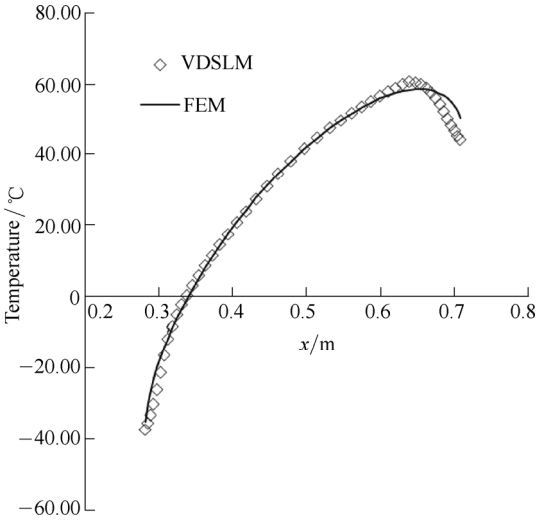

(a) Temperature along the upper side of the crack line

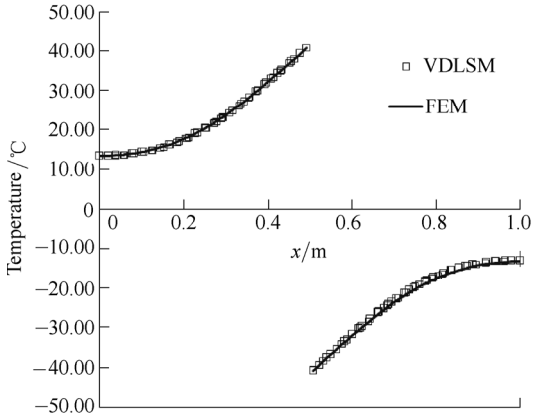

(b) Temperature along the line $y=0$

Fig. 19. Comparison of temperature distribution for the third problem

5.4 Steady-state heat conduction in a cylinder head

As the final example with an irregular shape containing concave boundaries, a part of a cylinder head of a Yamaha XS1100 engine was selected and modeled. A photo of such cylinder head was depicted in Fig. 20.

For minimizing the CPU RAM of computer during analysis, a central part of this cylinder head was considered and modeled. The nodal configurations used in VDLSM for this part of the cylinder head can be seen in Fig. 21.

The temperature on the external boundaries was considered as 400 ℃ and on the other internal boundaries was kept as 90 ℃. The thermal conductivity was considered as k=177.2 W/(m℃). Other required parameters for heat conduction solution are the same as the example 5.3. The number of used nodal points in VDLSM method was 3850. A second order polynomial shape functions with m=6 were implemented. Due to the lake of the analytical solution in this case, the obtained temperature distribution within the domain was compared with that obtained from ABAQUS standard software. Figs. 22 and 23 show this comparison.

Fig. 20. Yamaha XS1100 motor cylinder-head for the fourth problem

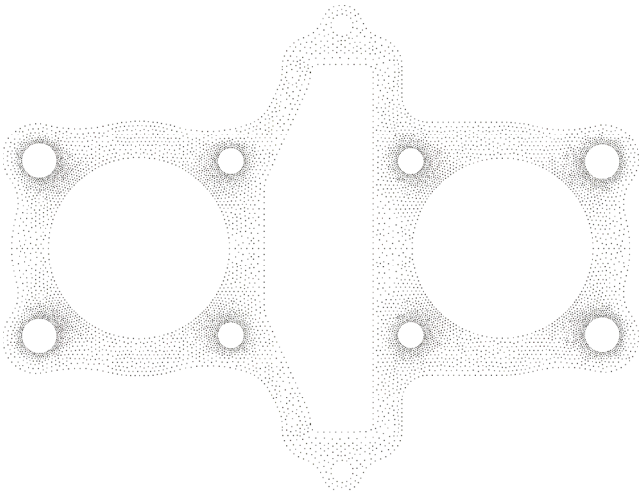

Fig. 21. Nodal configurations of the cylinder-head

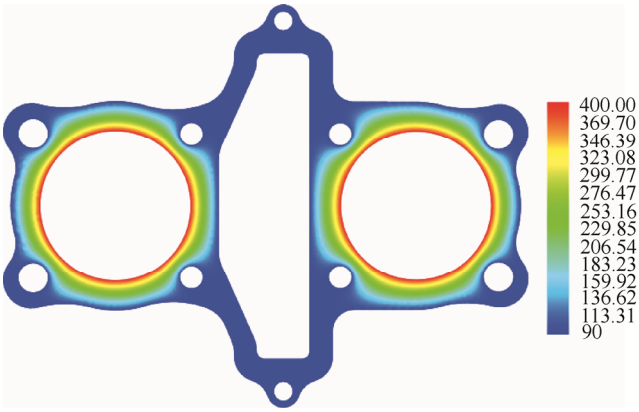

Fig. 22. Temperature contours (℃) for the cylinder-head predicted by VDLSM

In the FEM approach, 15 000 linear triangular heat transfer shell elements-DS3- of ABAQUS element library were used for modeling. It can be seen that there exists a

good correlation between these two kinds of results.

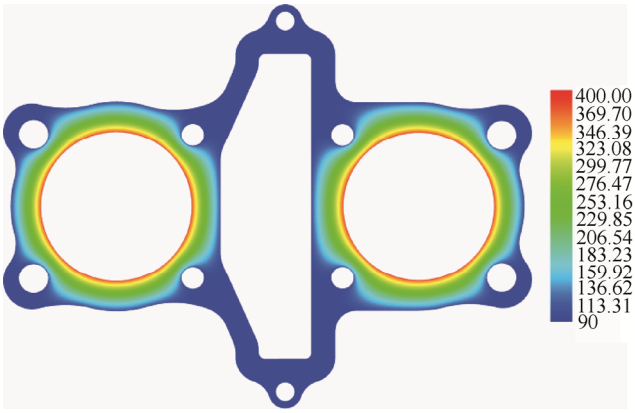

Fig. 23. Temperature contours (℃) for the cylinder-head predicted by F.E.M

6 Conclusions

(1) A modified discrete least square meshless method named as VDLSM is formulated and implemented for solving the steady-state heat conduction phenomenon in the domains contain crack or irregular concave boundaries.

(2)The advantages of the Voronoi tessellation algorithm is used for building up the support domains in such mentioned mediums precisely and subsequently for constructing weight and MLS shape functions.

(3)This method is a straight-forward scheme which does not suffer from the shortcomings of the other techniques such as visibility, diffraction or transparency. It guarantees the continuity condition for the shape functions; does not extend the time of processing, yields accurate results comparable with FEM and analytical results and high convergence rate for cracked domains or domains with highly irregular concave boundaries.

References

[1] GINGOLD R A, MONAGHAN J J. Smoothed particle hydrodynamics-theory and application to non-spherical stars[J]. *Mon Not* R*AstronSoc*, 1977,181: 375–389.

[2] LUCY L B. A numerical approach to the testing of the fission hypothesis[J]. *Astron. J*, 1977, 82: 1013–1024.

[3] NAYROLES B, TOUZOT G, VILLON P. Generalizing the finite element method: Diffuse approximation and diffuse elements[J]. *J Comp. Mech*, 1992, 10(5): 307–318.

[4] BELYTSCHKO T, LU Y Y, GU L. Element-free Galerkin methods[J]. *Int J Numer Meth Eng*, 1994, 37: 229–256.

[5] BELYTSCHKO T, KRONGAUZ Y, ORGAN D, et al. Meshless methods: an overview and recent developments[J]. *Comput Methods Appl Mech Engrg*, 1996, 139: 3–47.

[6] ZHANG X, PAN X F, HU W, et al. Meshless weighted least-square method[C]//*Proceeding of Fifth World Congress on Computational Mechanics,* Vienna, Austria, July 7–12, 2002.

[7] LIU W K, JUN S, ZHANG Y F. Reproducing kernel particle methods[J]. *Int J Numer Meth Fl*, 1995, 20: 1081–1106.

[8] ATLURI S, ZHU T. A new meshless local Petrov-Galerkin(MLPG) approach in computational mechanics[J]. *Comput Mech*, 1998, 22: 117–127.

[9] ATLURI S, ZHU T L. The meshless local Petrov-Galerkin(MLPG) approach for solving problems in elasto-statics[J]. *Comput Mech*, 2000, 25: 169–179.

[10] LIN H, ATLURI S. Meshless local Petrov-Galerkin(MLPG) method for convection diffusion problems[J]. *Comput Model Eng Sci*[J], 2000, 1: 45–60.

[11] CLEARY P W, MONAGHAN J J. Conduction modeling using smoothed particle hydrodynamics[J]. *J Comput Phys*, 1999, 148: 227–264.

[12] CHEN J K, BERAUN J E, CARNEY T C. A corrective smoothed particle method for boundary value problems in heat conduction[J]. *Int J Numer Meth Eng*, 1999, 46: 231–252.

[13] SADAT H, COUTURIER S. Performance and accuracy of a meshless method for laminar natural convection[J]. *Numer Heat Transfer Part B*, 2000, 37: 455–467.

[14] SADAT H, DUBUS N, GBAHOUE L, et al. On the solution of heterogeneous heat conduction problems by a diffuse approximation meshless method[J]. *Numer Heat Transfer Part B*, 2006, 50: 491–498.

[15] SOPHY T, SADAT H, PRAX C. A meshless formulation for three-dimensional laminar natural convection[J]. *Numer Heat Transfer Part B*, 2002, 41: 433–445.

[16] SINGH I V, SANDEEP K, PRAKASH R. Heat transfer analysis of two-dimensional fins using meshless element-free Galerkin method[J]. *Numer Heat Transfer A*, 2003, 44: 73–84.

[17] SINGH I V, SANDEEP K, PRAKASH R. The element free Galerkin method in three-dimensional steady-state heat conduction[J]. *Int J Comput Eng Sci*, 2002, 3: 291–303.

[18] SINGH I V, PRAKASH R. The numerical solution of three-dimensional transient heat conduction problems using element free Galerkin method[J]. *Int J Heat Tech*, 2003, 21: 73–80.

[19] SINGH A, SINGH I V, PRAKASH R. Numerical solution of temperature-dependent thermal conductivity problems using a meshless method[J]. *Numer Heat Transfer Part A*, 2006, 50: 125–145.

[20] SINGH I V. A numerical solution of composite heat transfer problems using meshless method[J]. *Int J Heat Mass Transfer*, 2004, 47: 2123–2138.

[21] YAN L, XIONG Z, MINGWAN L. Meshless least-squares method for solving the steady-state heat conduction equation[J]. *Tsinghua Sci Tech*, 2005, 10: 61–66.

[22] LIU Y, ZHANG X, LIU M W. A meshless method based on least-squares approach for steady-and unsteady-state heat conduction problems[J]. *Numer Heat Transfer*, 2005, 47: 257–275.

[23] CHENG R J, LIEW K M. A meshless analysis of three-dimensional transient heat conduction problems[J]. *Eng Anal Bound Elem*, 2012, 36: 203–210.

[24] SLADEK J, SLADEK V, ATLURI S N. Meshless local Petrov-Galerkin method for heat conduction problem in an anisotropic medium[J]. *Comput Model Eng Sci*, 2004, 6: 309–318.

[25] SLADEK J, SLADEK V, HON Y C. Inverse heat conduction problems by meshless local Petrov-Galerkin method[J]. *Eng Anal Bound Elem*, 2006, 30: 650–661.

[26] SLADEK J, SLADEK V, HELLMICH C H, et al. Heat conduction analysis of 3-D axisymmetric and anisotropic FCM bodies by meshless local Petrov-Galerkin method[J]. *Comput Mech*, 2007, 39: 323–333.

[27] QIAN L F, BaATRA R C. Three dimensional transient heat conduction in a functionally graded thick plate with a high order plate theory and a meshless local Petrov-Galerkin method[J]. *Comput Mech*, 2005, 35: 214–226.

[28] HONG W X, QUAN T W. Meshless method based on the local weak-forms for steady-state heat conduction problems[J]. *Int J Heat Mass Trans*, 2008, 51: 3103–3112.

[29] ARZANI H, AFSHAR M H. Solving Poisson's equations by the discrete least square meshless method[J]. *WIT Trans Model Simul*, 2006, 42: 23–31.

[30] FIROOZJAEE A R, AFSHAR M H. Discrete least squares meshless method with sampling points for the solution of elliptic partial differential equations[J]. *Eng Anal Bound Elem*, 2009, 33: 83–92.

[31] AFSHAR M H, LASHCKARBOLOK M, SHOBEYRI G. Collocated discrete least squares meshless(CDLSM) method for the solution of transient and steady-state hyperbolic problems[J]. *Int J Numer Meth Fl*, 2009, 60: 1055–1078.

[32] FIROOZJAEE A R, AFSHAR M H. Steady-state solution of incompressible Navier-Stokes equations using discrete least-squares meshless method[J]. *Int J Numer Meth Fl*, 2011, 67: 369–382.

[33] NAISIPOUR M, AFSHAR M H, HASSANI B, et al. Collocation discrete least square(CDLS) method for elasticity problems[J]. *Int J Civil Eng*, 2009, 7: 9–18.

[34] AMANI J, AFSHAR M H, NAISIPOUR M. Mixed discrete least squares meshless method for planar elasticity problems using regular and irregular nodal distributions[J]. *Eng Anal Bound Elem*, 2012, 36: 894–902.

[35] AFSHAR M H, NAISIPOUR M, AMANI J. Node moving adaptive refinement strategy for planar elasticity problems using Discrete Least Squares Meshless method[J]. *Finite Elem Anal Des*, 2011, 47: 1315–1325.

[36] AFSHAR M H, AMANI J, NAISIPOR M. A node enrichment adaptive refinement by Discrete Least Squares Meshless method for solution of elasticity problems[J]. *Eng Anal Bound Elem*, 2012, 36: 385–393.

[37] PIRALI H, DJAVANROOD F, HAGHPANAHI M. Combined visibility and surrounding triangles method for simulation of crack discontinuities in meshless methods[J]. *Journal of Applied Mathematics*, 2012, doi:10.1155/2012/715613.

[38] SUKUMAR N. Construction of polygonal interpolants: a maximum entropy approach[J]. *Int J Numer Meth Eng*, 2004, 61: 2159–2181.

[39] ORGAN D, FLEMING M, TERRY, T, et al. continuous meshless approximation for non convex bodies by diffraction and transparency[J]. *Computational Mechanics*, 1996, 18(3): 225–235.

[40] LINDSEY M, WESTOVER, SAMER M. Adeeb. Cubic spline meshless method for numerical analysis of the two-dimensional Navier-Stokes equations[J]. *International Journal of Numerical Analysis and modeling, Series B*, 2010, 1(2): 172–196.

[41] FLEMING M. *Element-Free Galerkin method for fatigue and quasi-static fracture*[D]. North–western University, June 1997.

[42] BUDAK BM, SAMARSKII A A, TIKHENEV A H. A collection of problems on mathematical physics[M]. translated by ARM Robson. New York: Pergamon Press, 1964, 331: 332–456.

Biographical notes

LABIBZADEH Mojtaba, born in 1976, is currently an assistant professor of structural engineering at *Civil Engineering Department, Faculty of Engineering, Shahid Chamran University, Ahvaz, Iran.* He received his bachelor and master degrees in civil engineering from *Shahid Chamran University, Ahvaz, Iran*, in 1999 and 2002 respectively. His research interests include numerical modeling, concrete constitutive modeling, and structural identification.

Tel: +98-613-330011; E-mail labibzadeh_m@scu.ac.ir